Multi-frequency Gaussian modeling of AGN jets with the extended Korean VLBI Network

Hyeon-Woo Jeong[1,2] and Sang-Sung Lee[1,2],
Whee Yeon Cheong[2], Sanghyun Kim[2], and Jae-Young Kim[3]

[1] *Astronomy and Space Science, University of Science and Technology*
[2] *Korea Astronomy and Space Science Institute*
[3] *Ulsan National Institute of Science and Technology*

Jets from AGNs

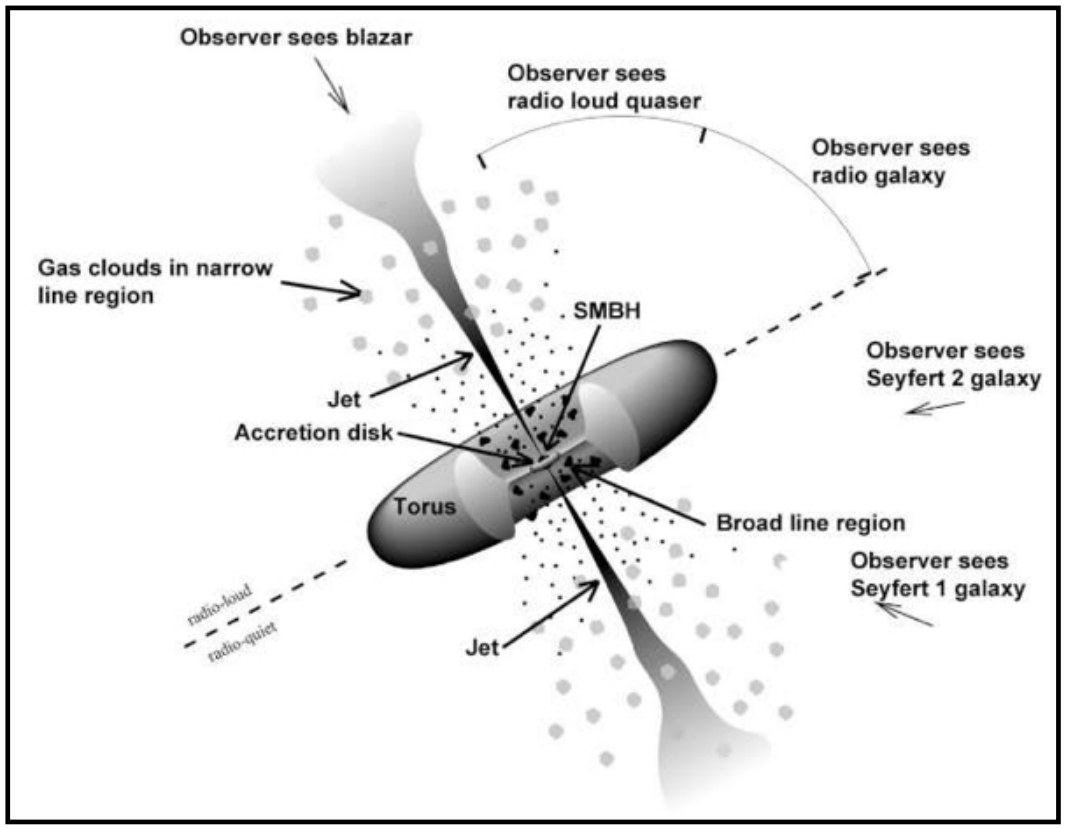

Mass accretion into the supermassive black hole

and ejection of plasma population

with relativistic speed

Cygnus A

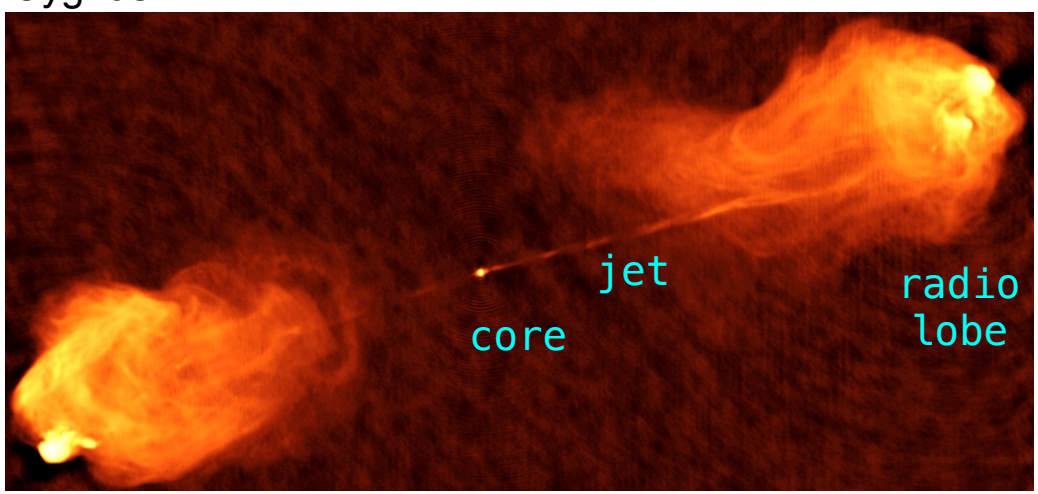

Jets from AGNs

Jet are resolved in VLBI observations
into several knot-features
in **VLBI** observations
&
when operated **at high frequencies**

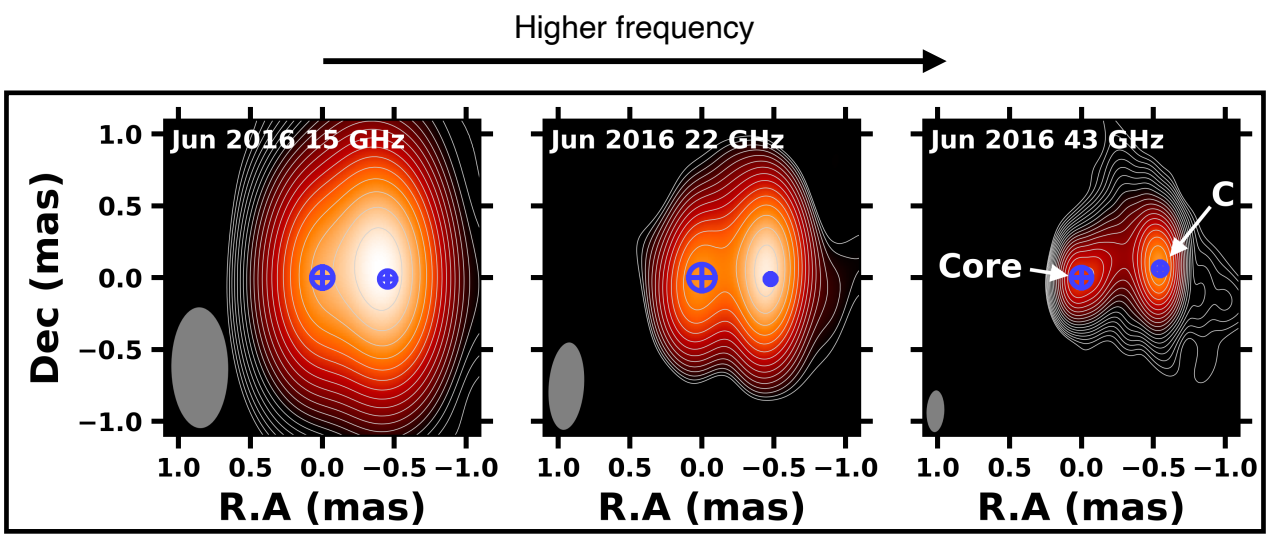

VLBA images of 3C 454.3 at 15—43 GHz
Jeong+2023

*mas: milli-arcsecond

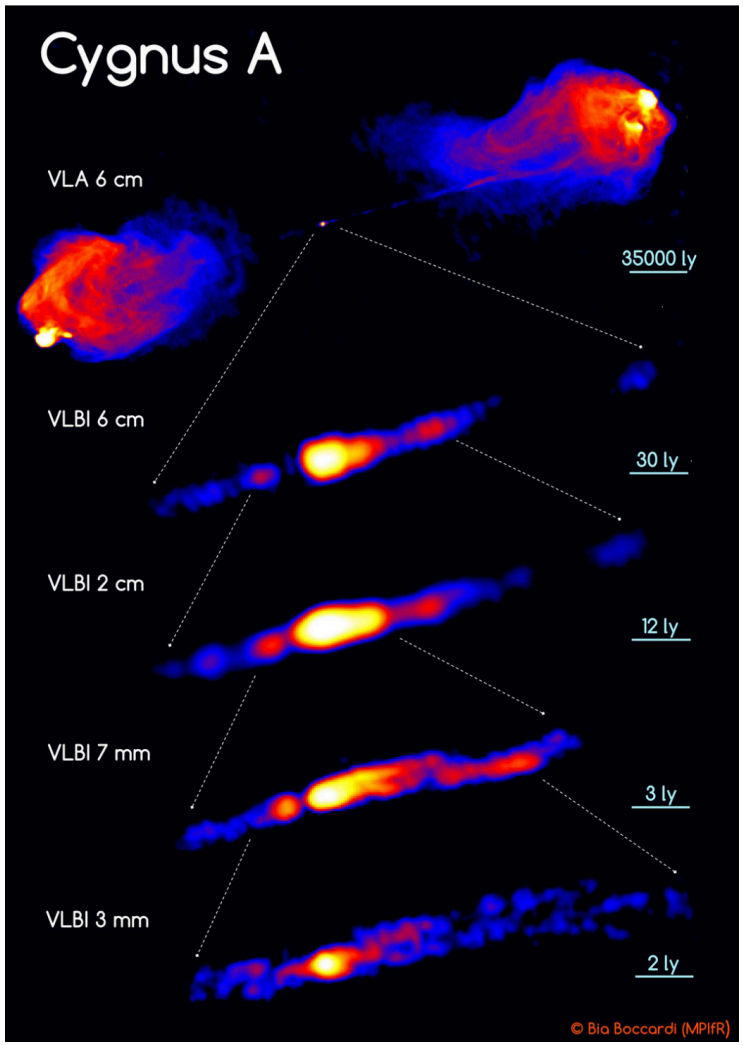

Boccardi+2017 (Rv)

Jets from AGNs

Jet are resolved in VLBI observations
into several knot-features
in **VLBI** observations
&
when operated **at high frequencies**

Mulit-frequency observaitons
provide valuable information of jets

(e.g., spectral index, Faraday rotation measure)

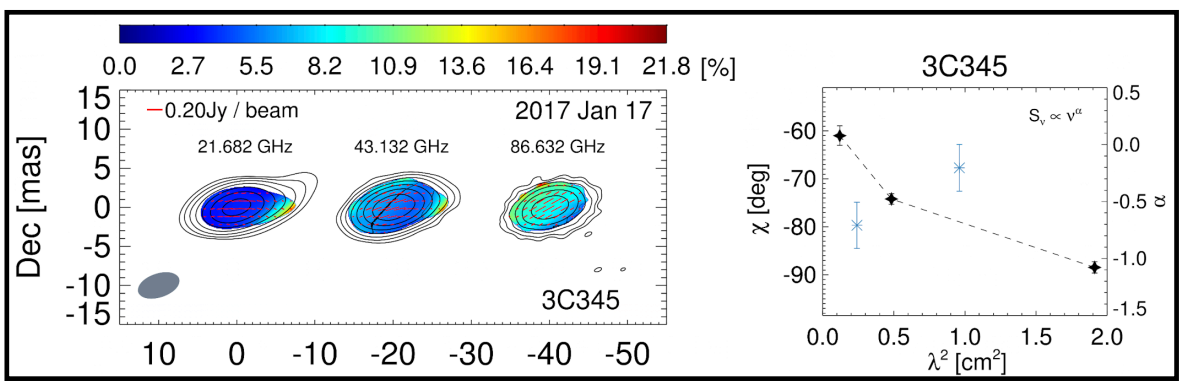

Degree of polarization and its angle of 3C 345, observed by the KVN (22 — 86 GHz)
Park+2018

Multi-frequency monitoring of KVN single-dish (MOGABA; Kang+2015)
on 3C 454.3 at 22—129 GHz (Jeong+2025)

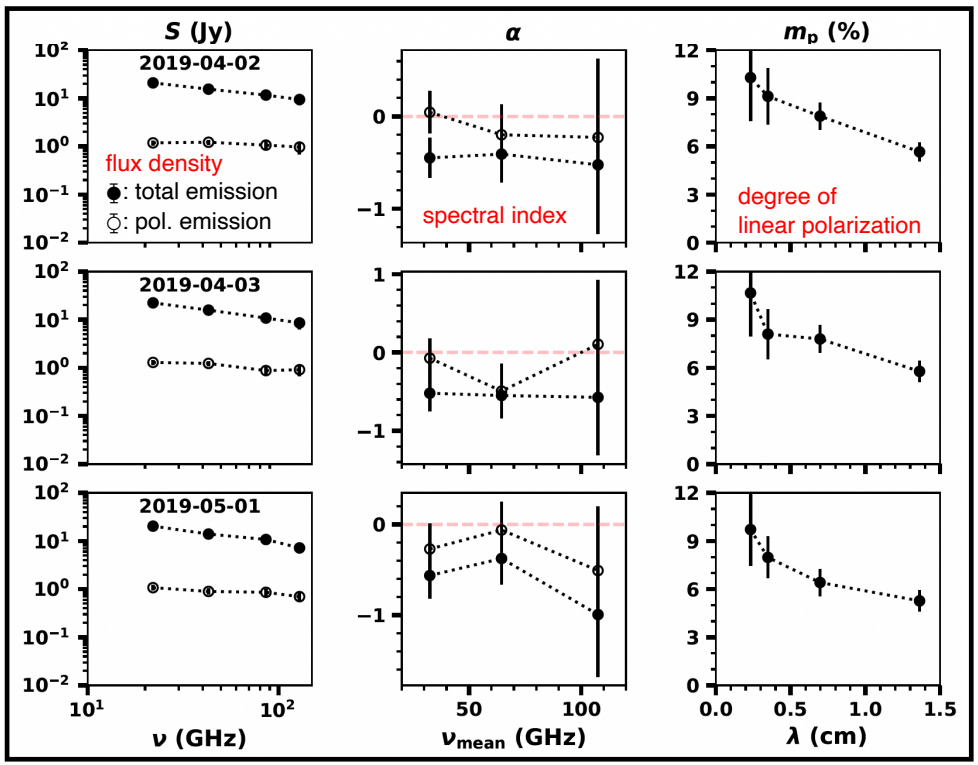

Why multi-frequency?

High-frequency observations are challenging due to **atmospheric fluctuations**, **decreasing coherence**, and low brightness of AGN jets

Coherence of an un-calibrated raw scan

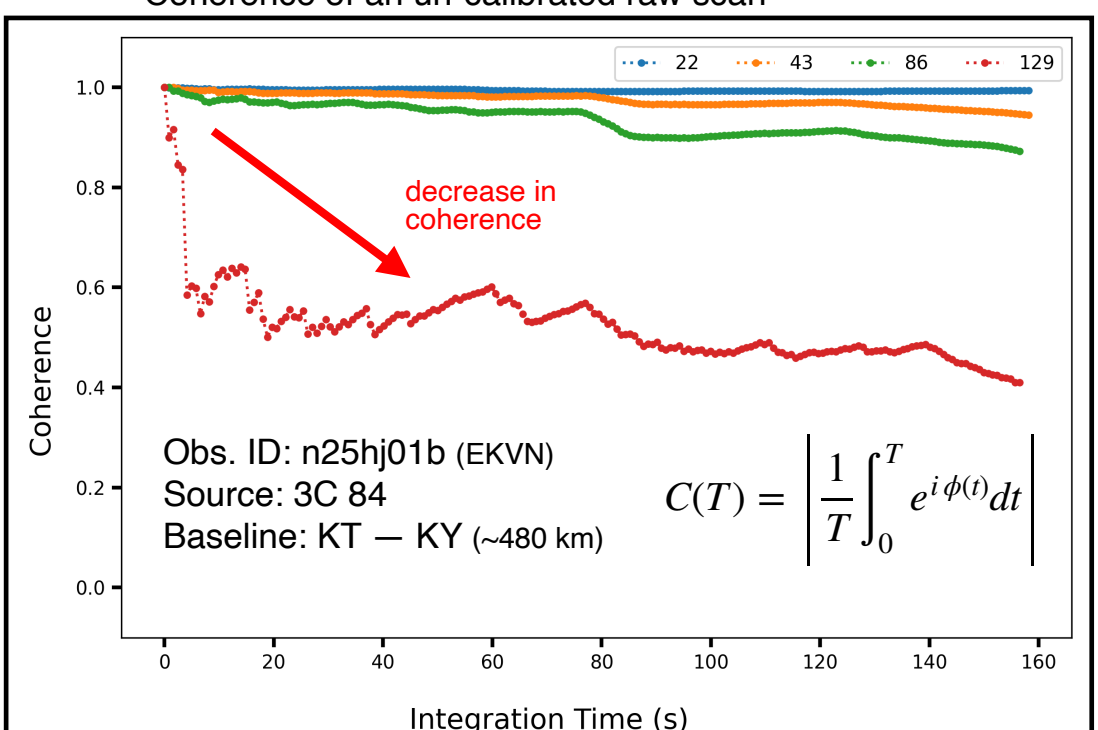

Multi-frequency monitoring of KVN single-dish (MOGABA; Kang+2015) on 3C 454.3 at 22—129 GHz (Jeong+2025)

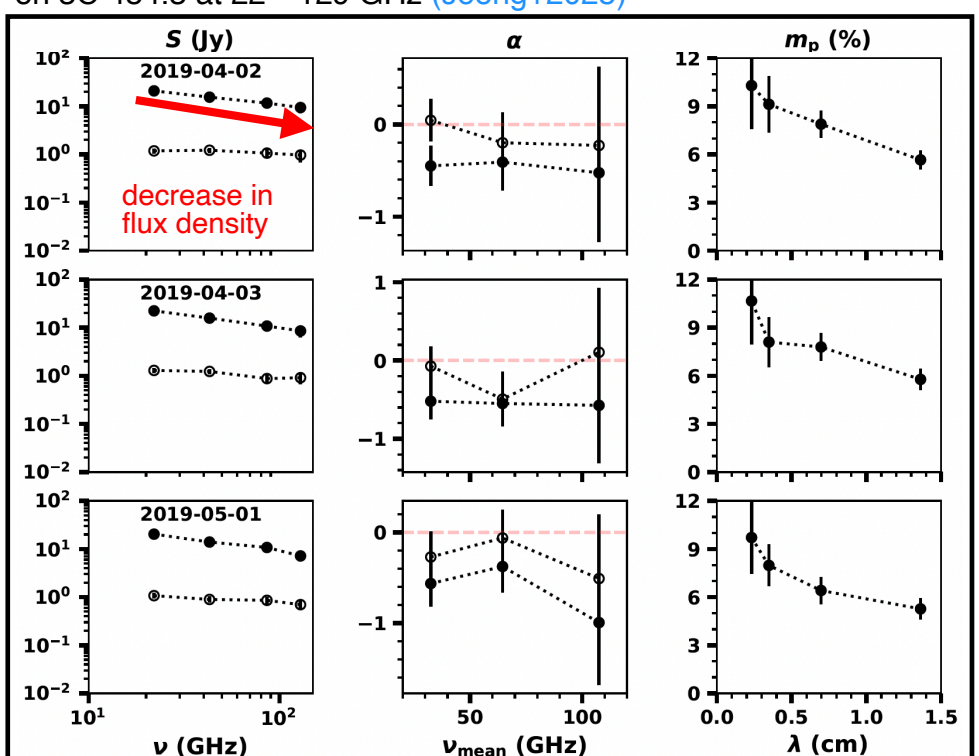

Why multi-frequency?

To improve coherence at high frequencies,
truely simultaneous multi-frequency capability is required
(i.e., frequency phase transfer; **FPT**; Rioja+2015)

Phase coherence at 215 GHz (Issaoun+2025)

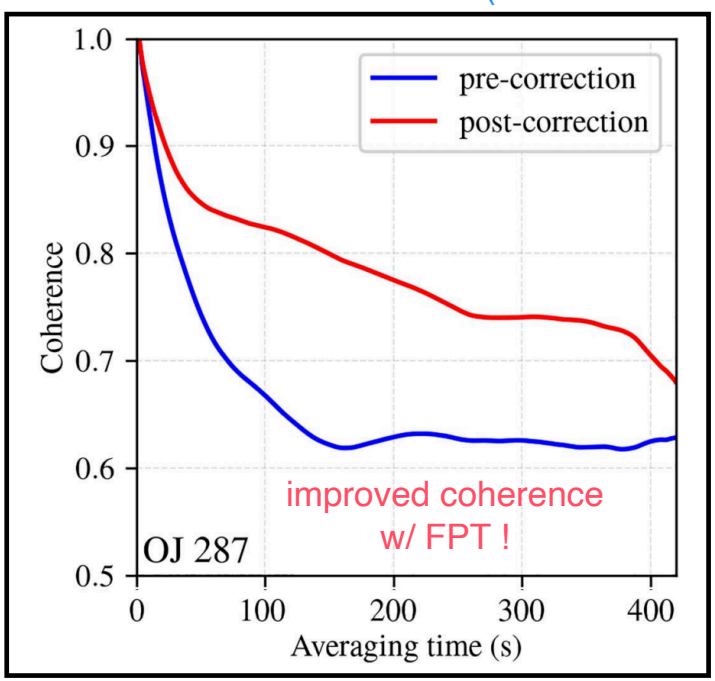

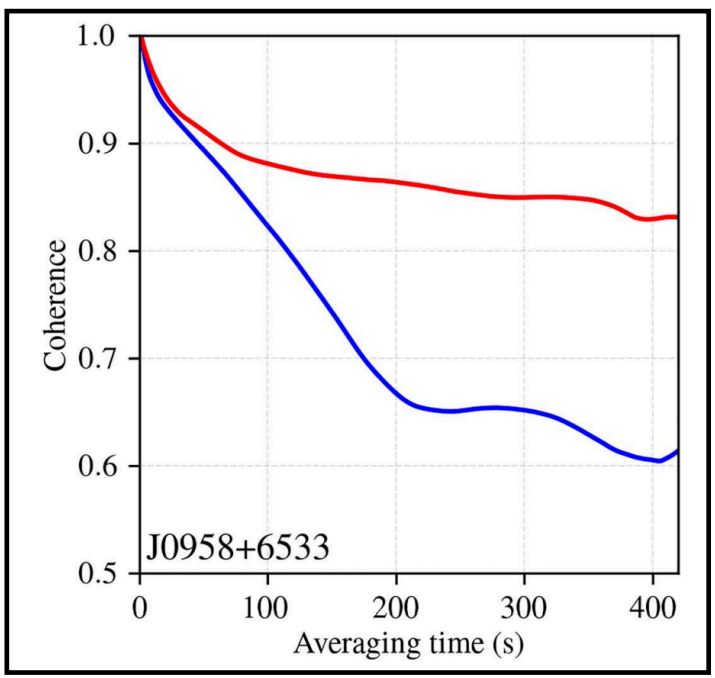

Extended Korean VLBI Network (EKVN)

KVN telescopes are equipped with simultanoues multi-frequency receiver

(typically, 22 – 129 GHz)

w/o FPT w/ FPT

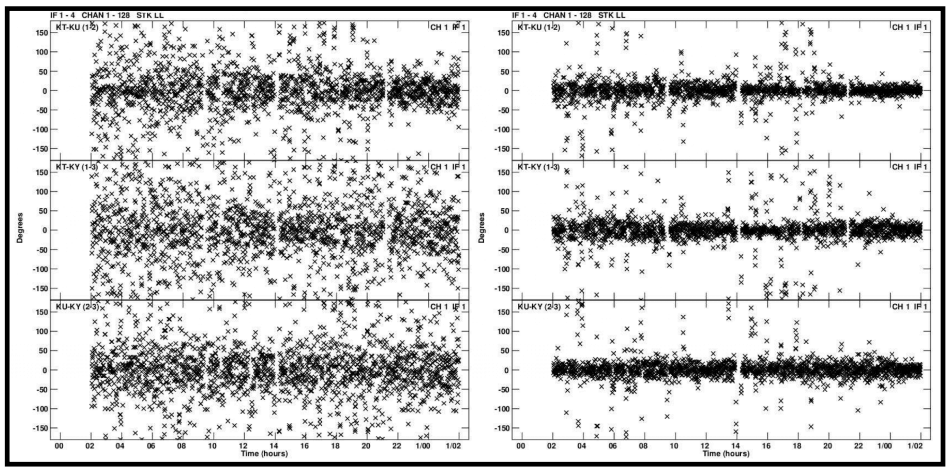

phase residuals, Hodgson+2016

A new station of the KVN at PyeongChang

(KPC / KC)

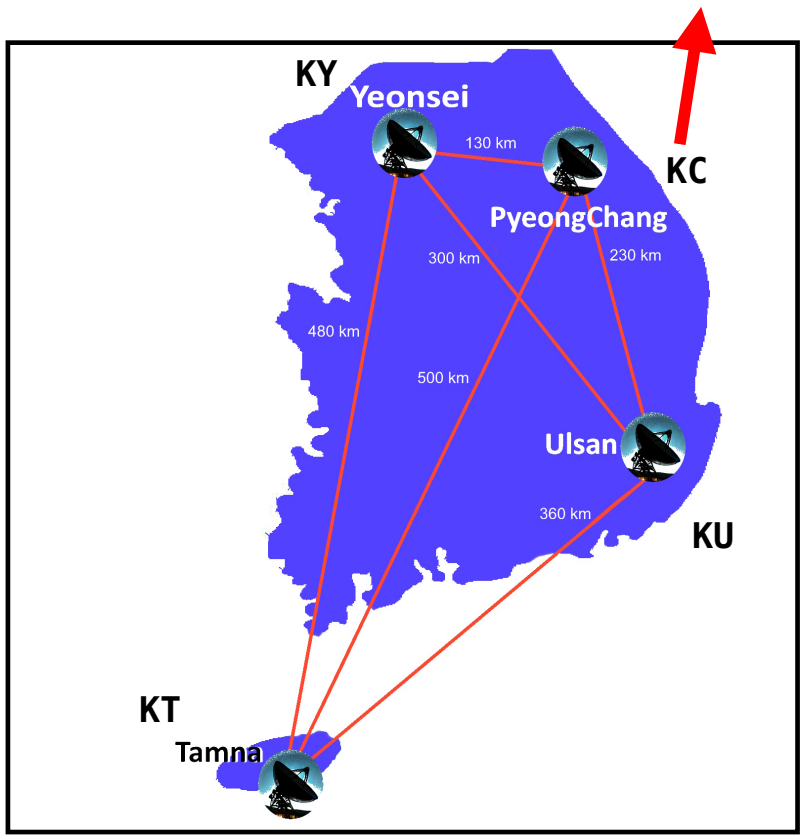

Multi-frequency synthesis (MFS)

Multi-frequency receiver enables the **MFS technique**

Through MFS, one can perform

1. **high angular resolution** analysis,
2. with the **increased sensitivity**
3. and the improved information through the combined **dense (u,v)-coverage**

* Data from the EKVN (3C 111, 2025-03-18)

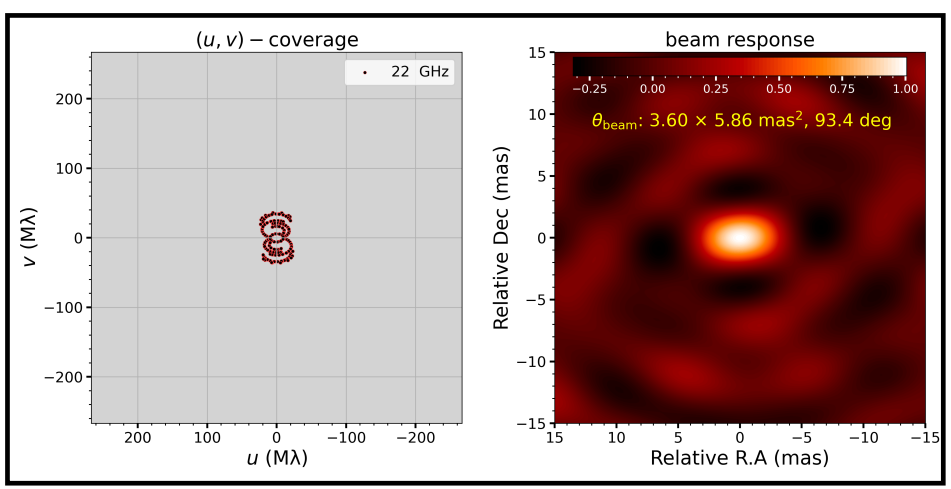

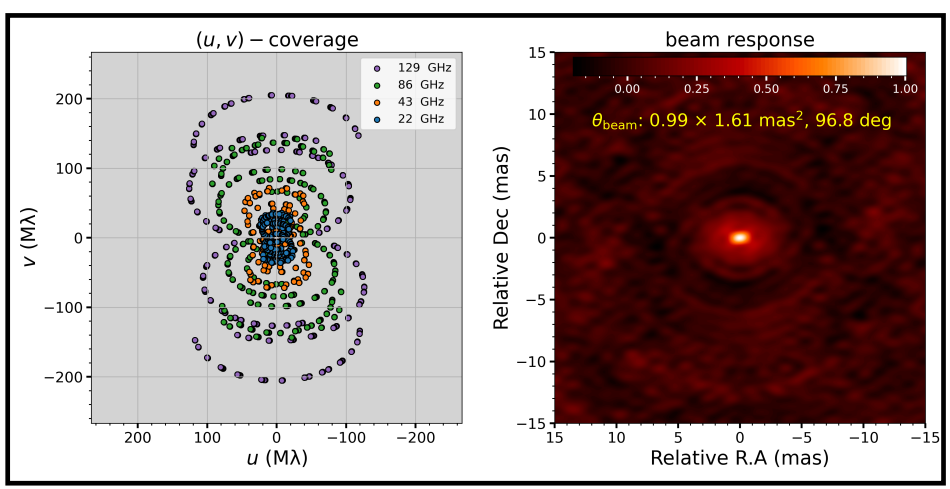

Gaussian multi-frequency modeling

Using the MFS and the assumptions below,
we developed a new modeling script,
Gaussian Multi-frequency VLBI Analyses (GaMVAs)*,
for AGN jets

* based on the python package, DYNESTY (Speagle 2020)

1. Jet morphology can be described by multiple 2D circular Gaussian model components

2. Common position of the Gaussian model components across frequencies

   - valid for optically thin jets

   - may not be valid for optically thick core
     (e.g., core-shift effect ≤ 0.1 mas, at 22–43 GHz; Pushkarev+2019, Chamani+2023, Benke+2025)

   - nevertheless, may be valid for those in the EKVN images
     ($B_{min,129}$ ~ 0.6 mas)

Gaussian multi-frequency modeling // complex visibility of a multi-frequency Gaussian

1. Complex visibility in a baseline : $\mathscr{V}(u,v) = \iint I(l,m)\, e^{-2\pi i(ul+vm)}\, dl\, dm$

→ circular Gaussian : $\mathscr{V}_m(u,v;\theta') = S\, e^{-2\pi a^2(u^2+v^2)}\, e^{2\pi i(ul_0+vm_0)}$
(single frequency)

$\theta' = (S,\ a,\ l_0,\ m_0)$

S : flux density [Jy]
a : angular size [mas]
l_0 : right ascension offset [mas]
m_0 : declination offset [mas]

2. Synchrotron self-absorption : $S(\nu; S_\mathrm{m}, \nu_\mathrm{m}, \alpha) = S_\mathrm{m} \left(\frac{\nu}{\nu_\mathrm{m}}\right)^{2.5} \times \frac{1-\exp(-\tau_\mathrm{m}(\nu/\nu_\mathrm{m})^{\alpha-2.5})}{1-e^{-\tau_\mathrm{m}}}$

(Turler+1999)

3. Multi-frequency Gaussian : $\mathscr{V}_m(u_\nu, v_\nu, \nu; \theta) = S(\nu; S_\mathrm{m}, \nu_\mathrm{m}, \alpha) \times e^{-2\pi a^2(u_\nu^2+v_\nu^2)} e^{2\pi i(u_\nu l_0 + v_\nu m_0)}$

$\theta = (S,\ a,\ l_0,\ m_0,\ \alpha,\ \nu_\mathrm{m})$

α : spectral index
ν_m : turnover frequency [GHz]
ν : observing frequency [GHz]

Gaussian multi-frequency modeling // antenna-gain-free closure relations

1. Observed visibility :

$$\widetilde{\mathcal{V}}_{12} \equiv \widetilde{A}_{12} e^{i\widetilde{\phi}_{12}} \approx A_{g1}A_{g2}A_{12}\, e^{i(\phi_{12}+\phi_{g1}-\phi_{g2})} + n_{\rm t}$$

A_{ij} : visibility amplitude [Jy]

ϕ_{ij} : visibility phase [rad]

$n_{\rm t}$: random thermal noise

$\mathcal{G}_1 := A_{g1}e^{\phi_{g1}}$: complex gain of antenna 1

2. Closure amplitude :

$$\mathcal{A}_{1234} = \frac{|\widetilde{\mathcal{V}}_{12}||\widetilde{\mathcal{V}}_{34}|}{|\widetilde{\mathcal{V}}_{13}||\widetilde{\mathcal{V}}_{24}|} \approx \frac{|A_{g1}A_{g2}||A_{g3}A_{g4}|}{|A_{g1}A_{g3}||A_{g2}A_{g4}|}\,\frac{|A_{12}||A_{34}|}{|A_{13}||A_{24}|} = \frac{A_{12}A_{34}}{A_{13}A_{24}}$$

3. Closure phase :

$$\begin{aligned}\psi_{123} &= \widetilde{\phi}_{12} + \widetilde{\phi}_{23} + \widetilde{\phi}_{31} \\ &\approx (\phi_{12} + \phi_{g1} - \phi_{g2}) \\ &\quad +(\phi_{23} + \phi_{g2} - \phi_{g3}) \\ &\quad +(\phi_{31} + \phi_{g3} - \phi_{g1}) = \phi_{12} + \phi_{23} + \phi_{31}\end{aligned}$$

Gaussian multi-frequency modeling // objective function, optimal number of models

1. Modeling script aims to minimize **Bayesian information crietria (BIC)**

$$\mathrm{BIC} = k\ln(n) - 2\ln(\mathscr{L})$$

k : degree of freedom

n : the number of data points

2. Likelihood $\mathscr{L}$ with independent normal Gaussian noise is given by

$$\mathscr{L} = \prod_{i=1}^{n} \frac{1}{\sqrt{2\pi\sigma_i^2}} \exp\left(-\frac{1}{2}\left(\frac{\mathrm{model}_i - \mathrm{data}_i}{\sigma_i}\right)^2\right)$$

σ_i : uncertainty of i^{th} data

then, $$\mathrm{BIC} = k\ln(n) + \sum_{i=1}^{n}\left[\left(\frac{\mathrm{model}_i - \mathrm{data}_i}{\sigma_i}\right)^2 + \ln(2\pi\sigma_i^2)\right]$$

Observation // n25hj01a

Obs. date: 2025 02-10 06:00 – 02-11 06:00 (24h)
Bands: 22 / 43/ 86 / 129 GHz
Sources: 21 AGNs

0235+164	1226+023 (3C 273)
0316+413 (3C 84)	1228+126 (M 87)
0415+379 (3C 111)	1253−055 (3C 279)
0420−014	1510−089
0430+052 (3C 120)	1553+113
0446+112	1641+399 (3C 345)
0735+178	1652+398 (Mrk 501)
0851+202 (OJ 287)	1749+096
0954+658	1807+698 (3C 371)
1156+295 (Ton 599)	2200+420 (BL Lac)
	2251+158 (3C 454.3)

Broad distribution in vis. amplitude caused by technical issue at 22 GHz during the observation

* red vertical lines: 99% level

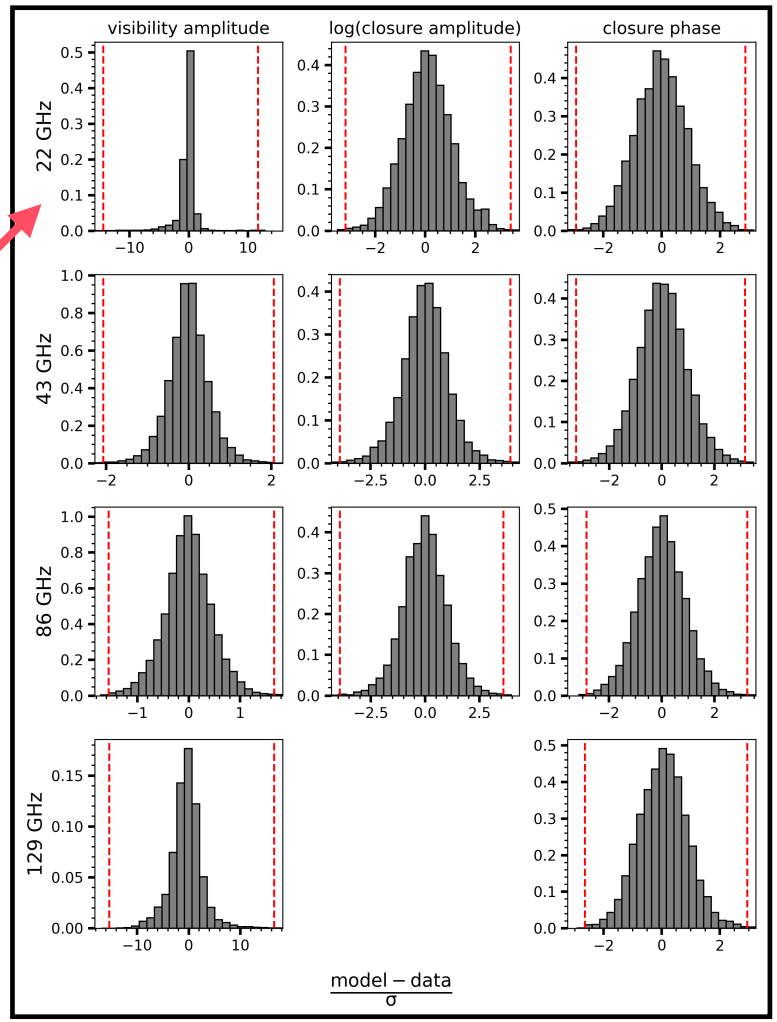

Normalized residual distribution obtained from all modeling results, except for 3C 84

Modeling results

Representative sources: **3C 111** & 3C 345

$\nu_{\mathrm{m,core}} = 40.4 \pm 2.4$ GHz
$\alpha = -0.58 \pm 0.05$

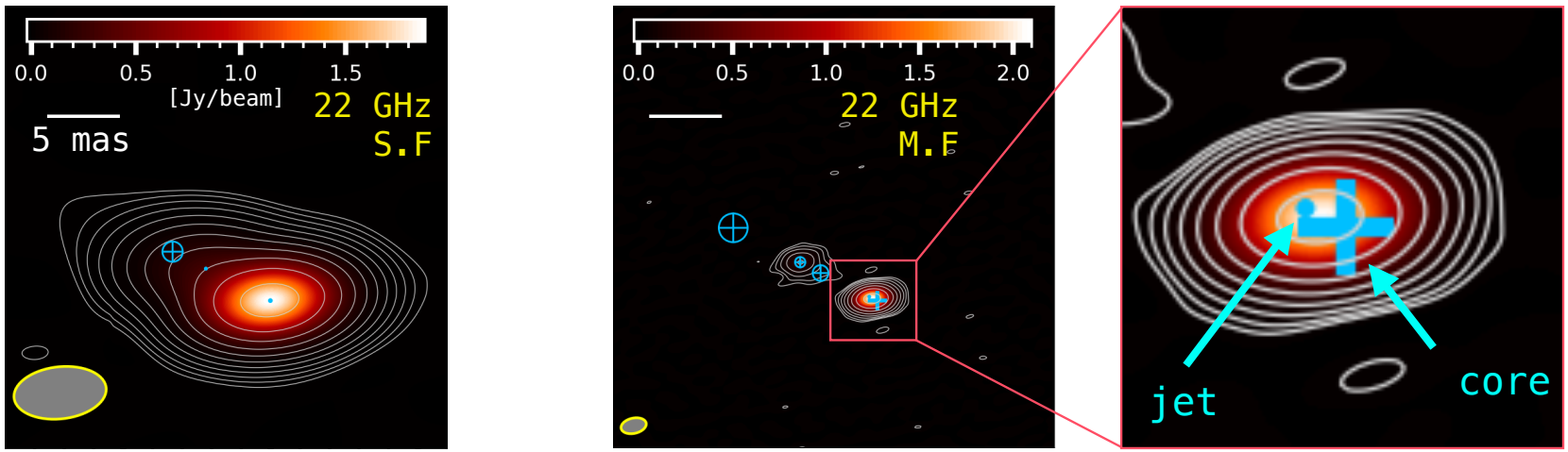

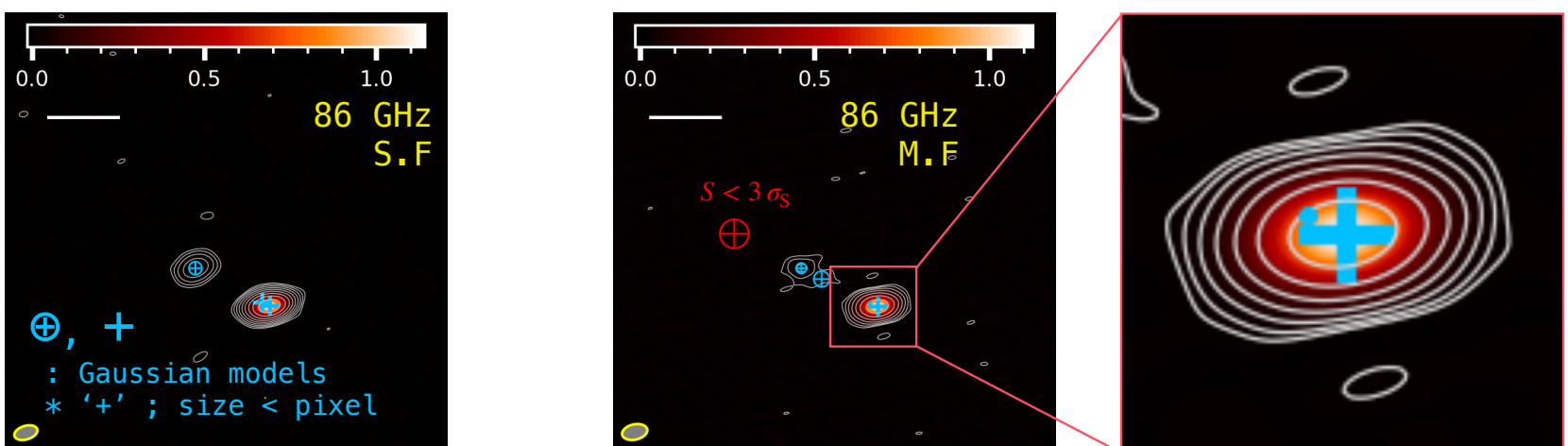

*
residual noise maps
are obtained from
DFT of
residual visibility

Modeling results

Representative sources: 3C 111 & **3C 345**

$\nu_{\mathrm{m,core}} = 23.2 \pm 0.4$ GHz
$\alpha = -0.73 \pm 0.01$

** for this source, there are only records of three stations at 22 GHz (technical issue at KPC)

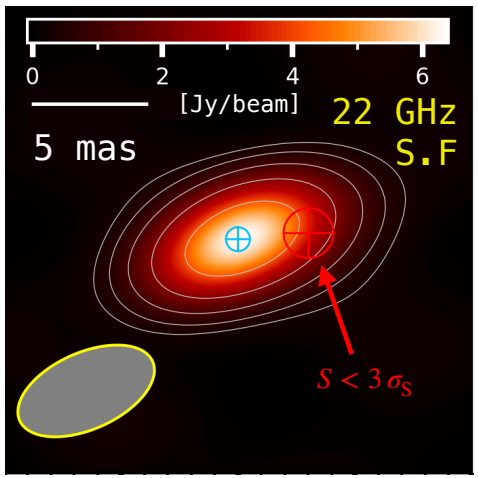

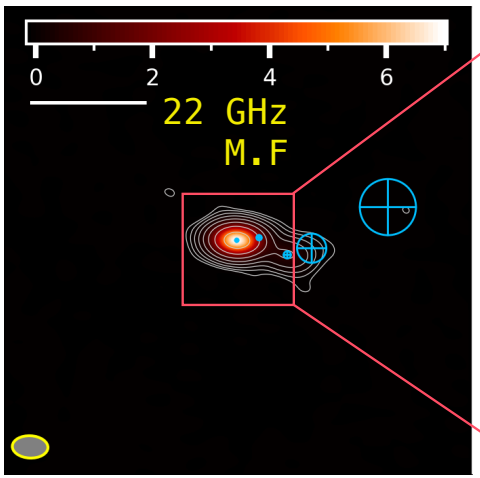

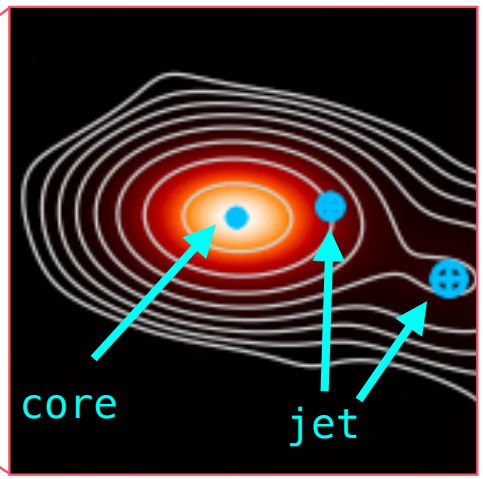

* residual noise maps are obtained from DFT of residual visibility

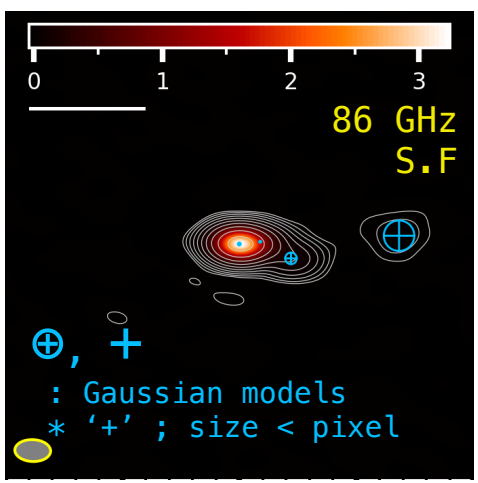

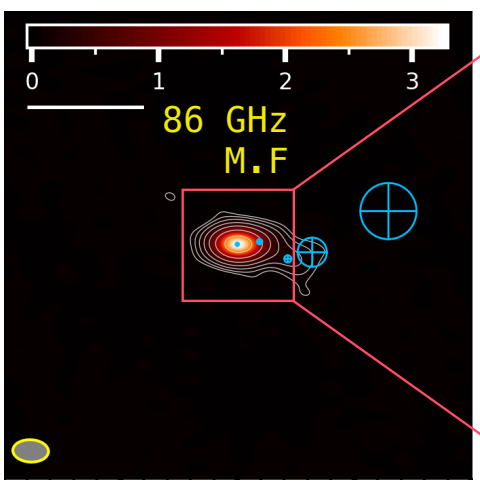

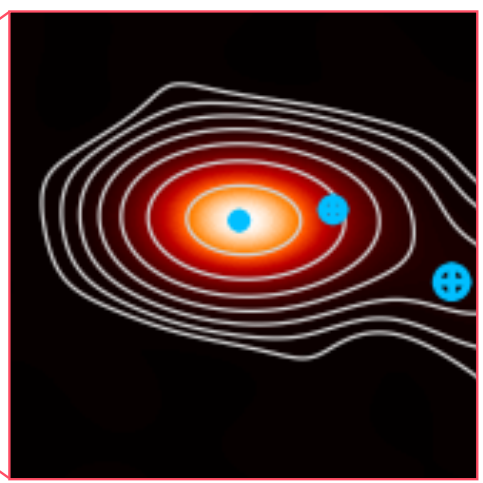

Compare with uv-radius-limited VLBA at 43 GHz

(u,v)−coverage
(≤ 200 Mλ, VLBA)

VLBA
(2025−02−16)

EKVN
(2025−02−10)

normalized cumulative
flux density
(43 GHz)

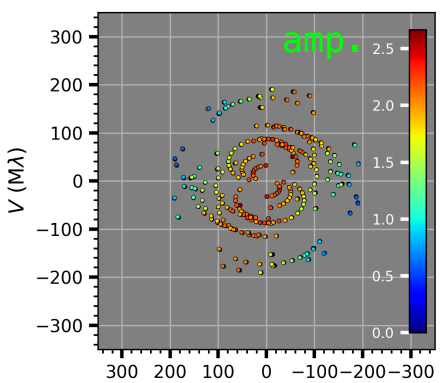

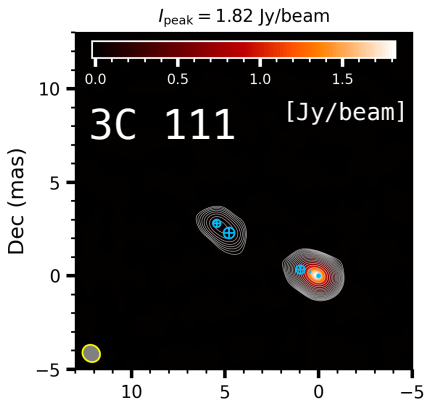

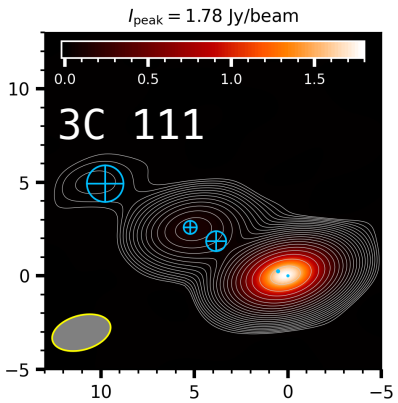

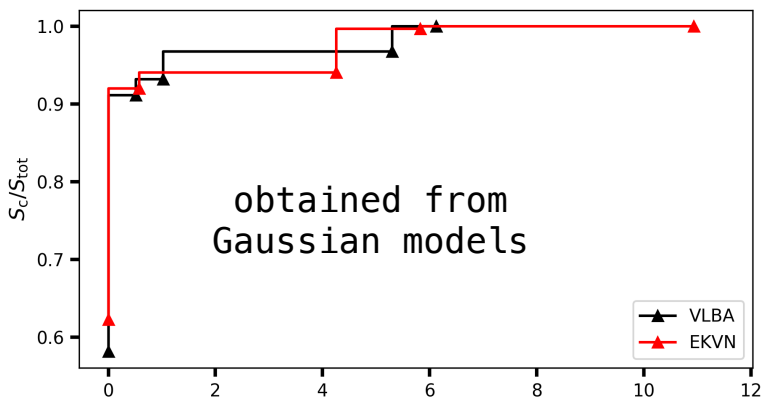

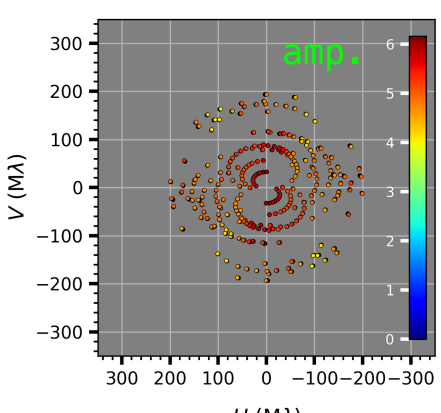

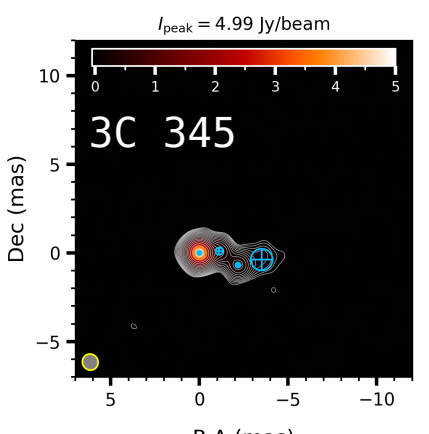

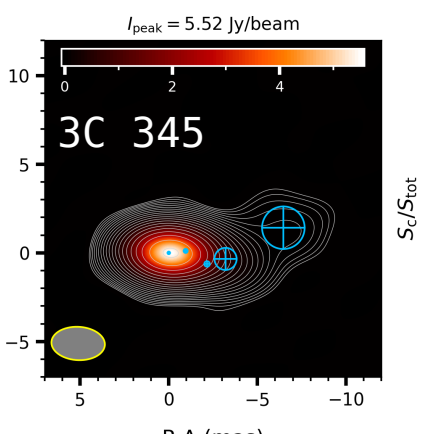

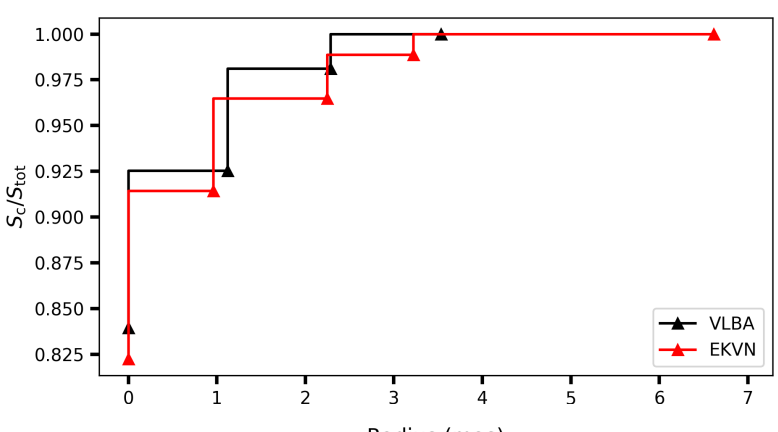

Reconstruction on extended jet (22 GHz, n25hj01b, 2025-03-18)

The short baseline length of the KC station
enables detection on **large-scale jets** & its polarization

3C 273 | 3C 345 | Mrk 501 | 3C 454.3

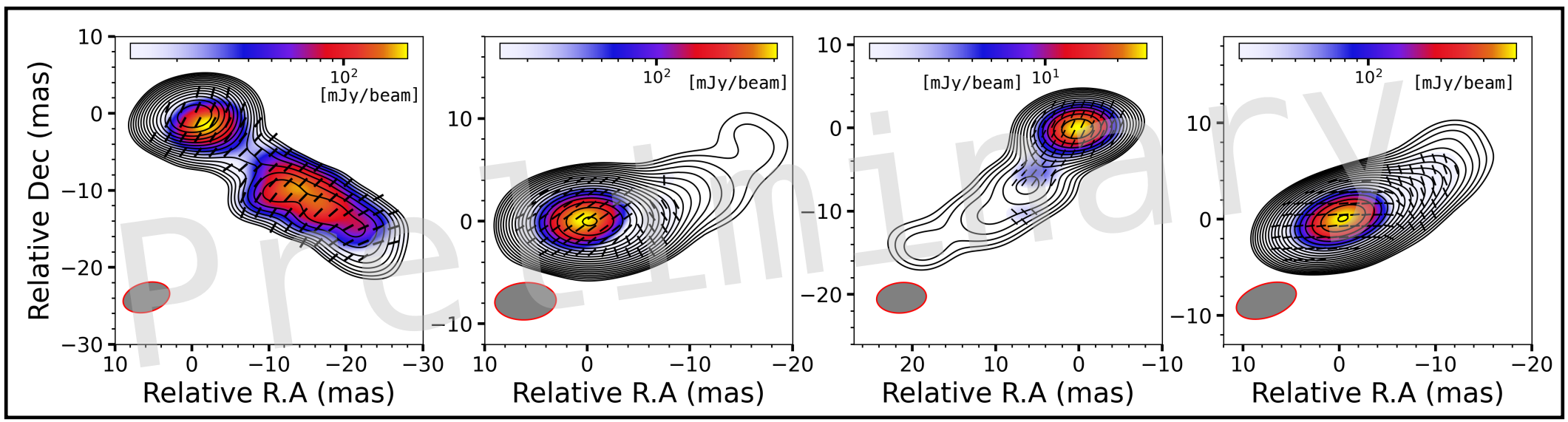

*NOTE: obtained from CLEAN images

Further scientific analysis?

Physical evolution along the jet

e.g.,
brightness temperature,
spectral index,
Faraday rotation measure,
…

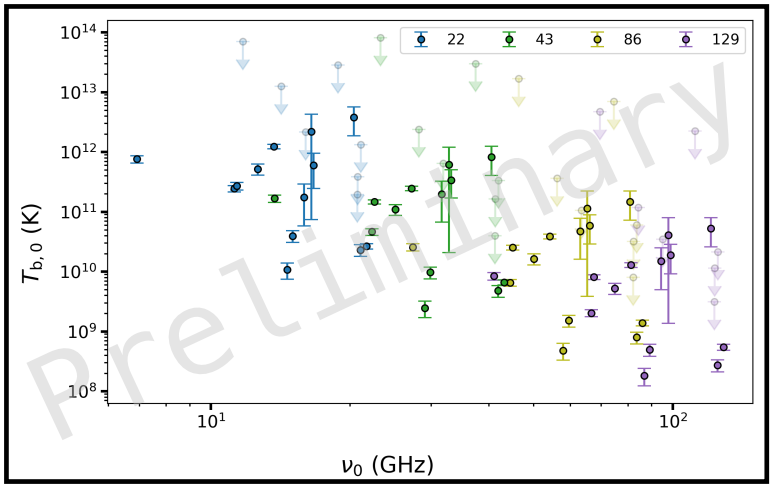

observed brightness temperature of cores (source rest frame)

* $\nu_0 = \nu_{\rm obs}/(1+z)$

Faraday rotation measure of 3C 273 along jet (**19 – 22 GHz**, n25hj02b, 2025-03-18)

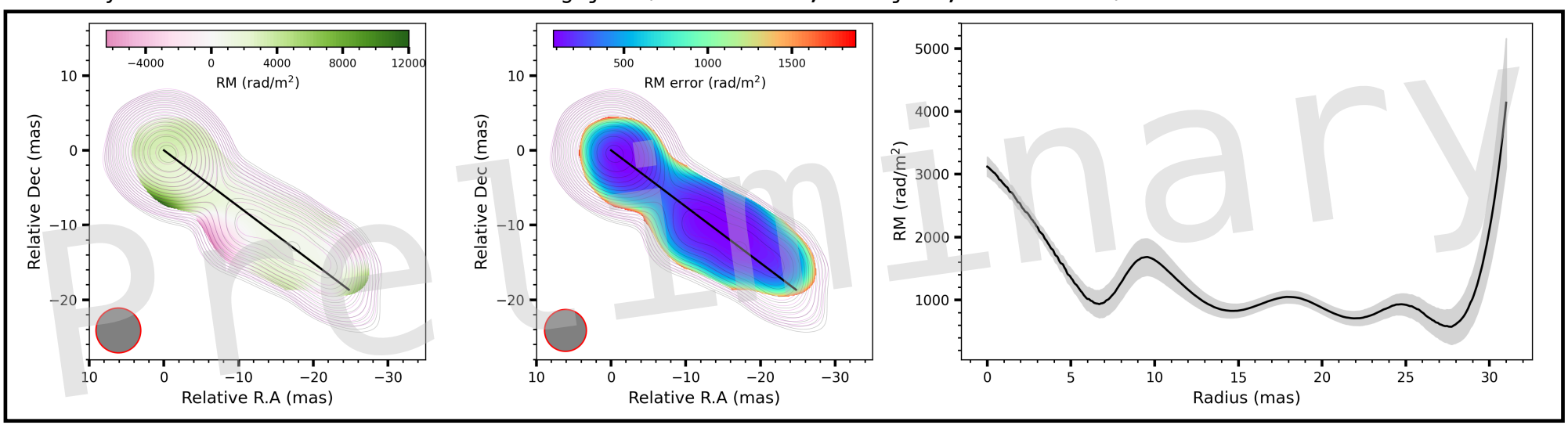

*NOTE: obtained from CLEAN images

Summary

- Truely simultaneous multi-frequency receiver is crucial for increasing high-frequency coherence

- MFS technique enables us to use higher angular resolution and sensitivity, resolving inner jet morphology within the EKVN resolution

- Our modeling scheme using the GaMVAs yields acceptable statistics and comparable modeling results with uv-limited VLBA

Thank you

Supplementary

Systematics // median absolute deviation (MAD), Mrk 501 @ 43 GHz (supplementary)

assumption: normally-distributed closure relations (SNR > 3)

$$\mathrm{mad}(Y) = 1.483\ \mathrm{med}(|Y|) = 1.483\ \mathrm{med}\left(\frac{|X - X_{\mathrm{med}}|}{\sigma}\right) = 1$$

original

MAD-corrected

log. closure amplitude

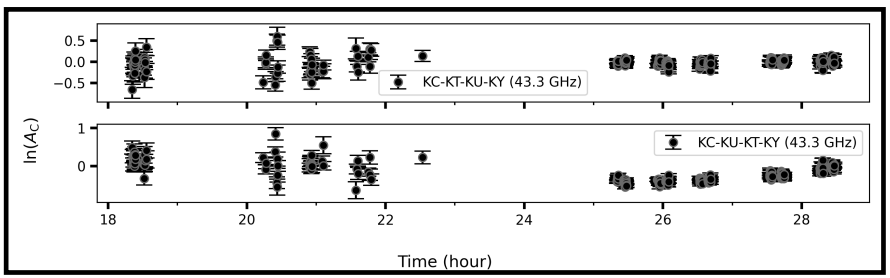

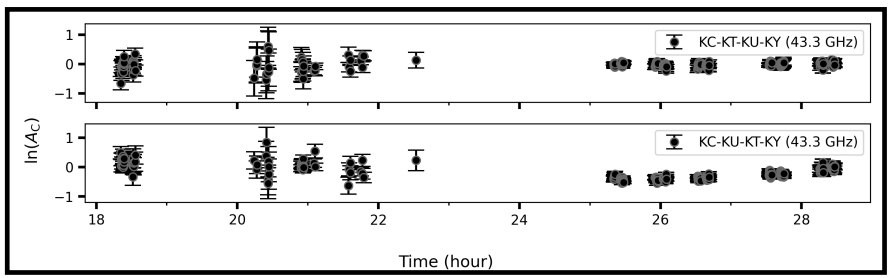

closure phase

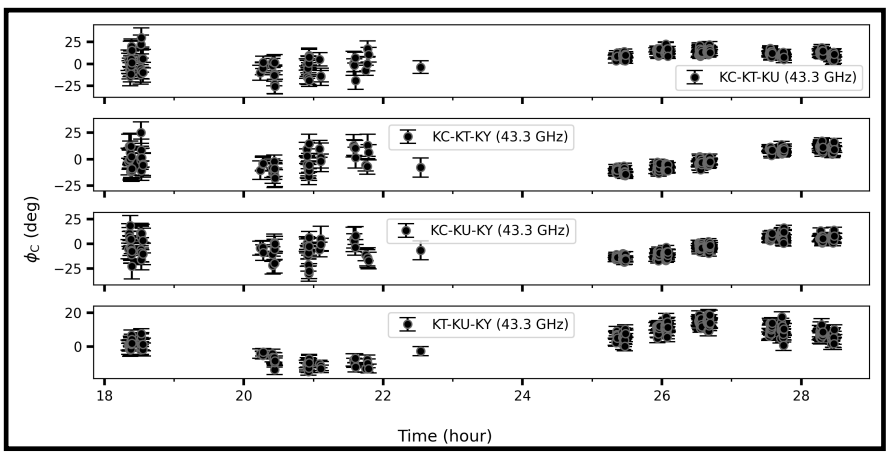

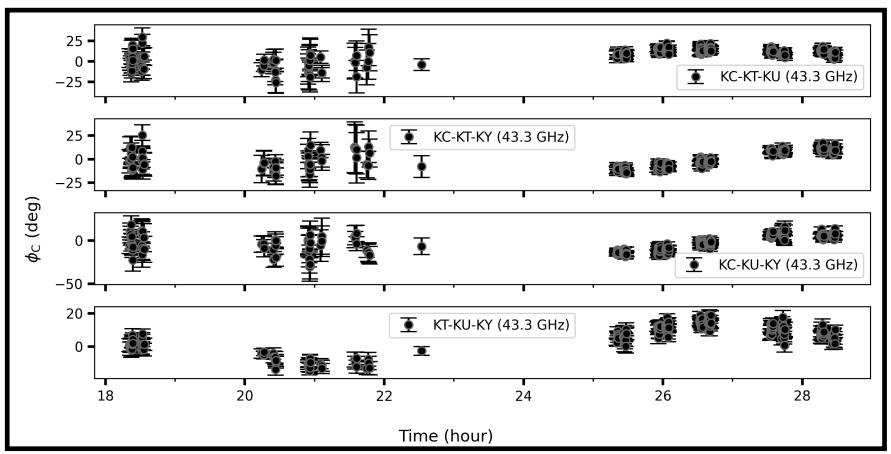

Observation // n25hj01a, technical issue (supplementary)

probably induced by clock synchronization

KC	KT	KU	KY
PPSGAP @ K-band (+ Q-band, unknown) 00-16:53:18 – 01-00:57:42	PPSGAP @ K-band 01-00:19:47 – 01-01:18:44	clear	late start due to freq. setup 00:06:52:00 –

For KC-baselines,
no-fringe @ K-band
weaker fringe @ Q-band

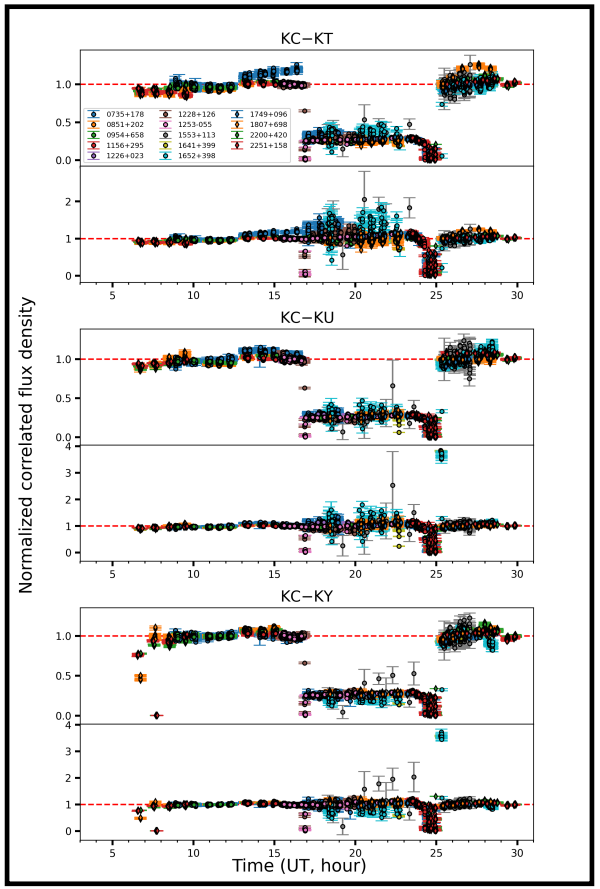

Normalized vis. amplitude of KC-baselines
upper: w/o correction
lower: w/ correction

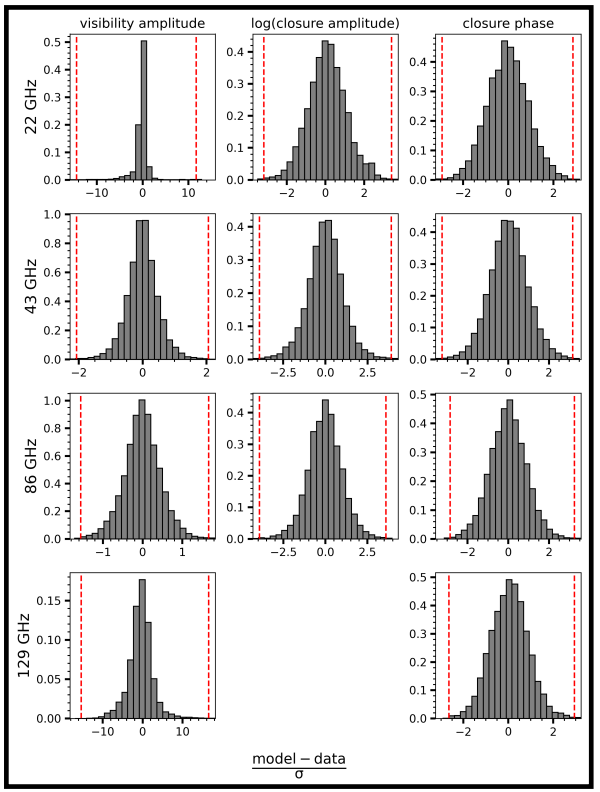

Broader normalized residual in logarithmic closure amplitude
→ affected by the systematics

Error estimation from posterior distributions // (supplementary)

* NOTE:
first model
is fixed to (0,0)
in the map

3C 111
(core comp.)

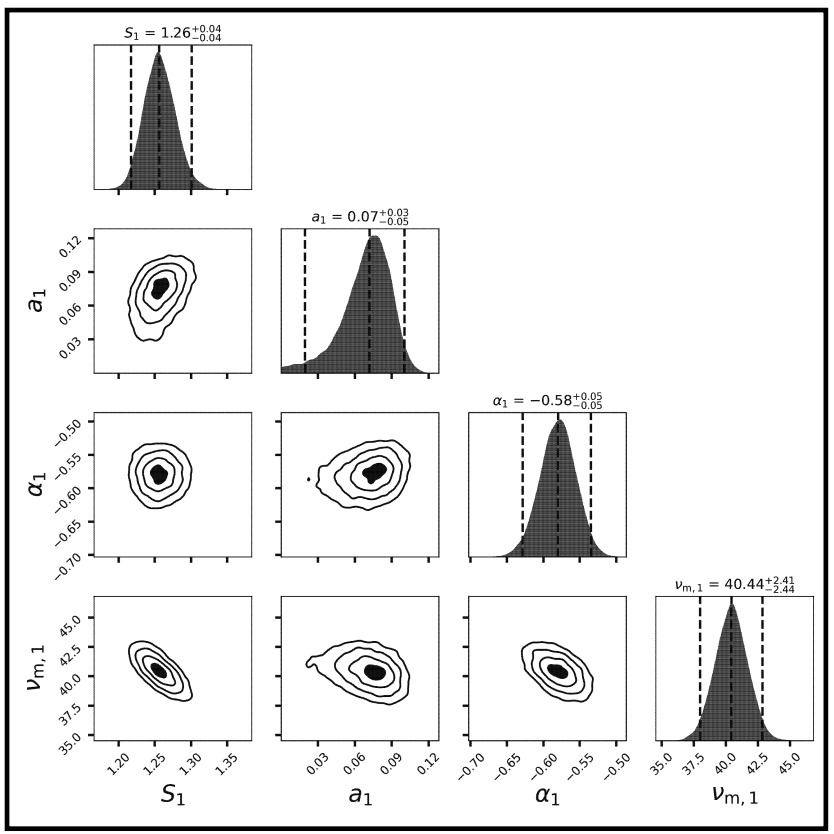

flux density (Jy) | size (mas) | spectral index ($S \propto \nu^{\alpha}$) | turnover freq. (GHz)

3C 345
(core comp.)

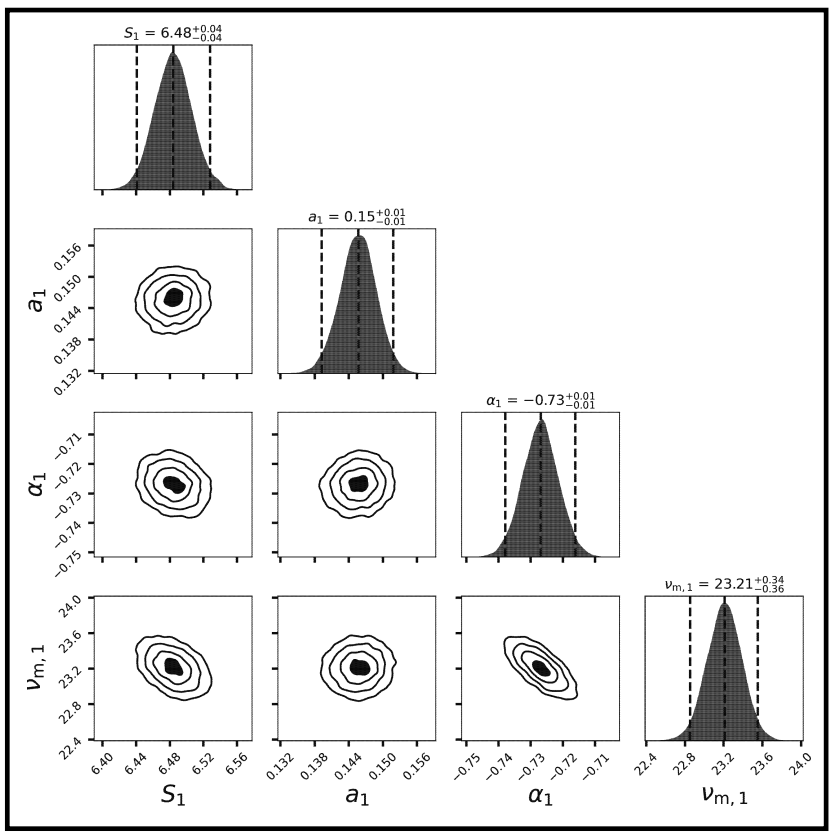

flux density (Jy) | size (mas) | spectral index ($S \propto \nu^{\alpha}$) | turnover freq. (GHz)

Pros and cons // (supplementary)

Pros

- Dense sampling on (u,v)-plane through the MFS technique
- Antenna-gain-independent closure quantities during modeling, which are not supported in DIFMAP
- Direct error estimation from posterior distribution, provided by the Bayesian modeling
- Characteristic physical parameters from Gaussian modeling

Cons

- Lack of deeper considertaion to the core-shift effect
- Inflexibility in spectrum model (e.g., free-free absorption or synchrotron aging)
- Insufficient criteria for the goodness of the model fitting
- Expensive computational cost

Modeling results // closure relations (supplementary)

Source: 3C 111 (logarithmic closure amplitude)

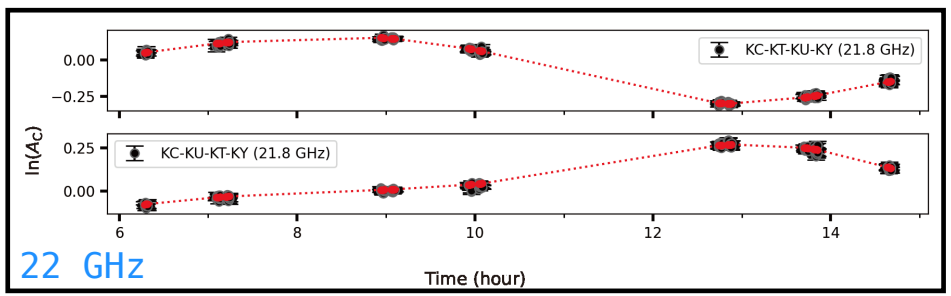

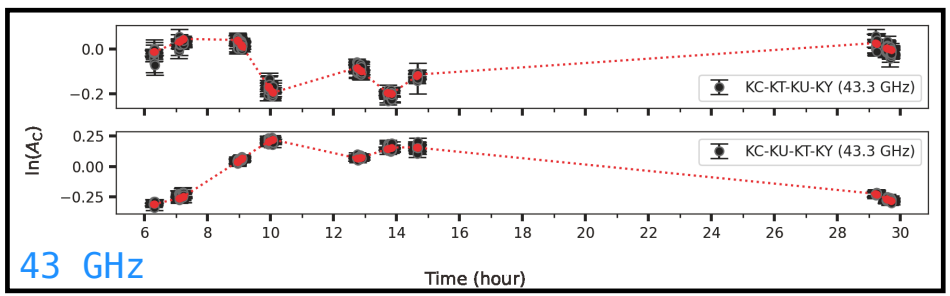

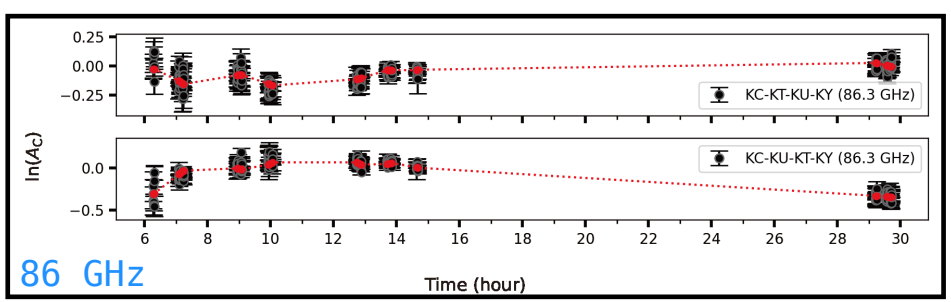

129 GHz: None of Cl. amp
(only 3 stations)

Modeling results // closure relations (supplementary)

Source: 3C 111 (closure phase)

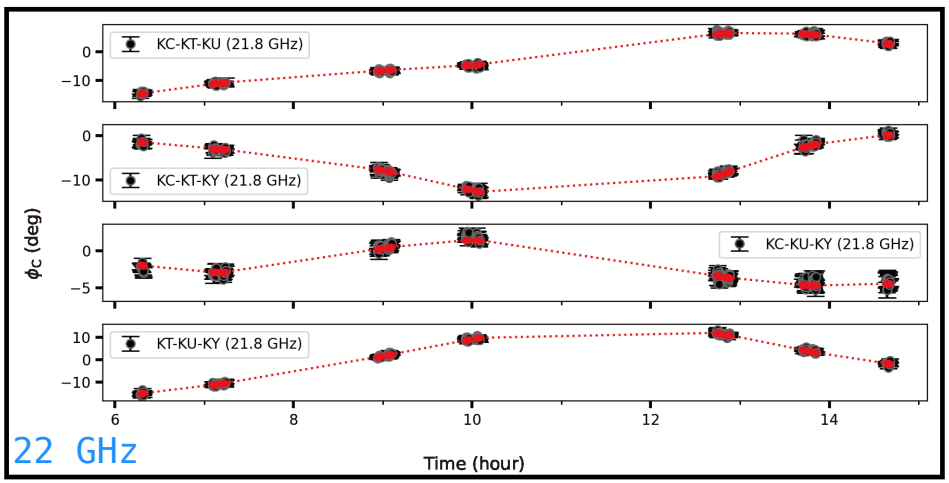

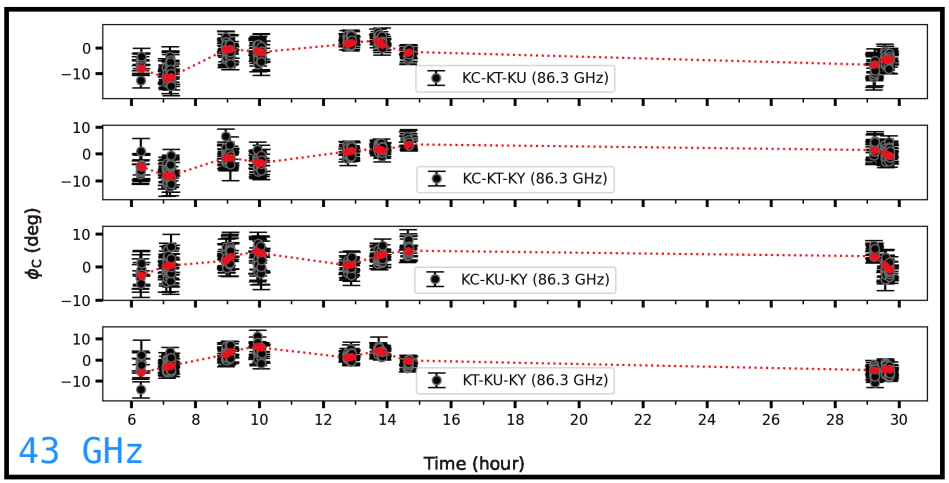

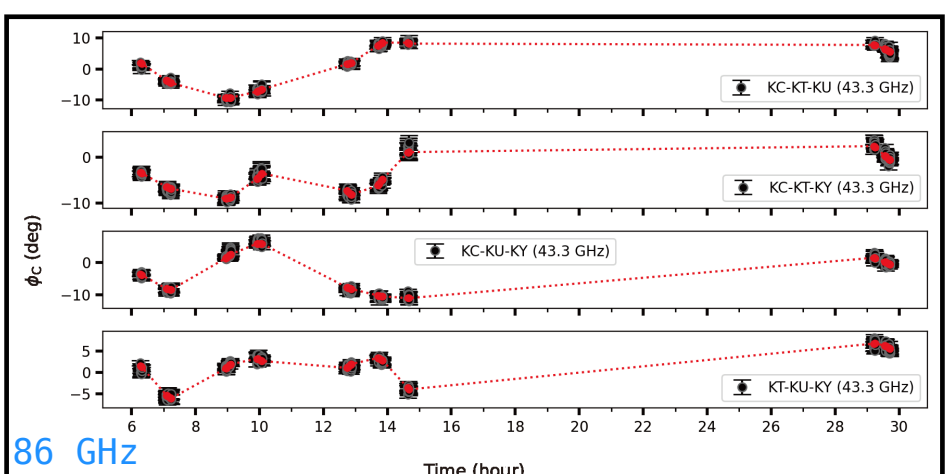

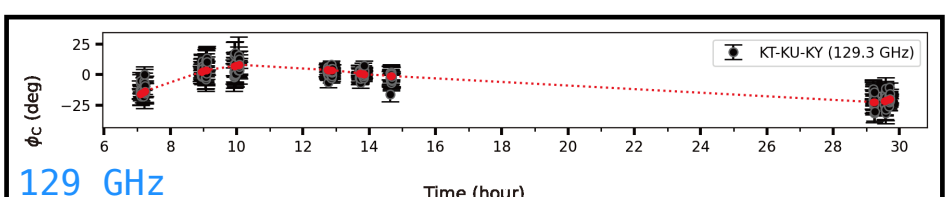

Modeling results // closure relations (supplementary)

Source: 3C 345 (logarithmic closure amplitude)

22 GHz: None of Cl. amp
(only 3 stations)

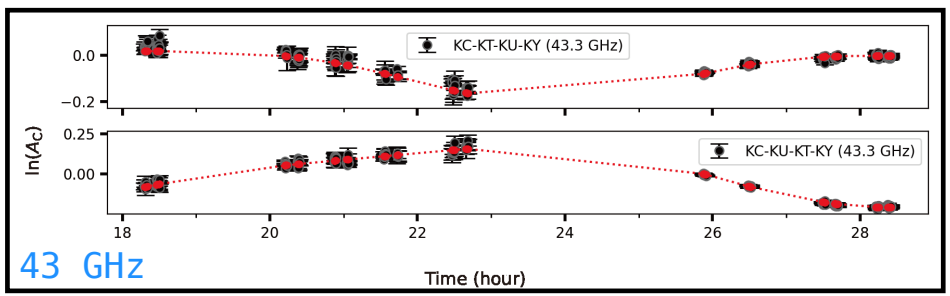

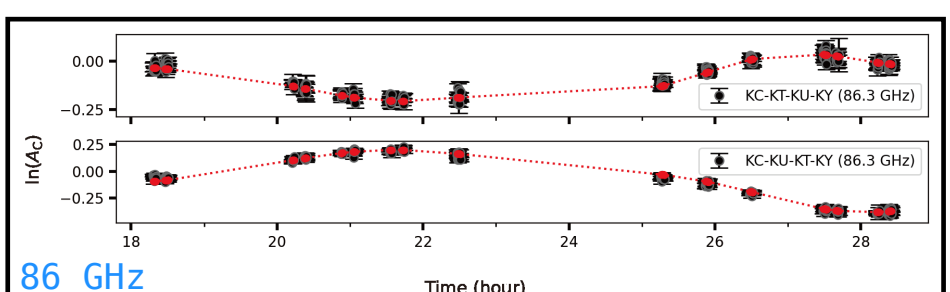

129 GHz: None of Cl. amp
(only 3 stations)

Modeling results // closure relations (supplementary)

Source: 3C 345 (closure phase)

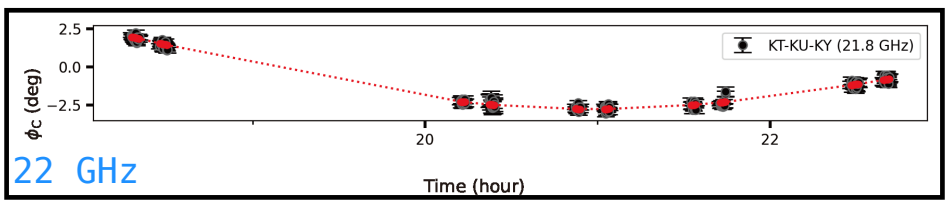

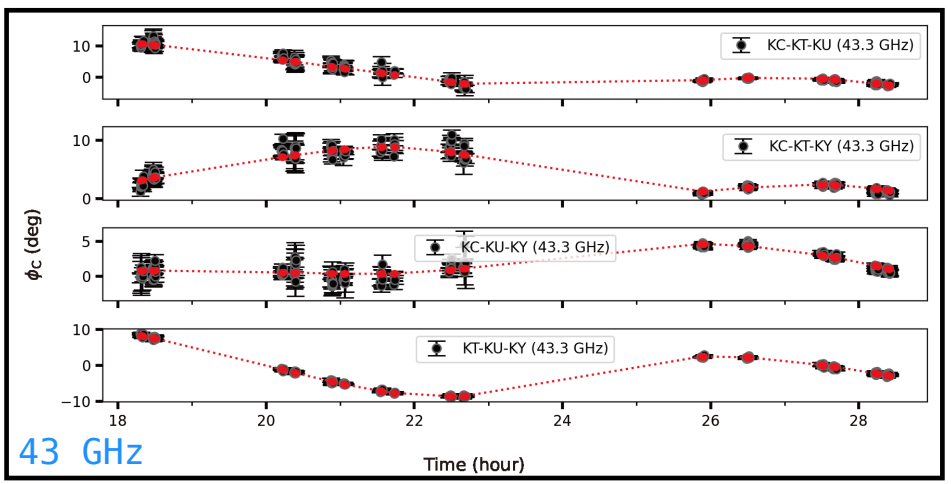

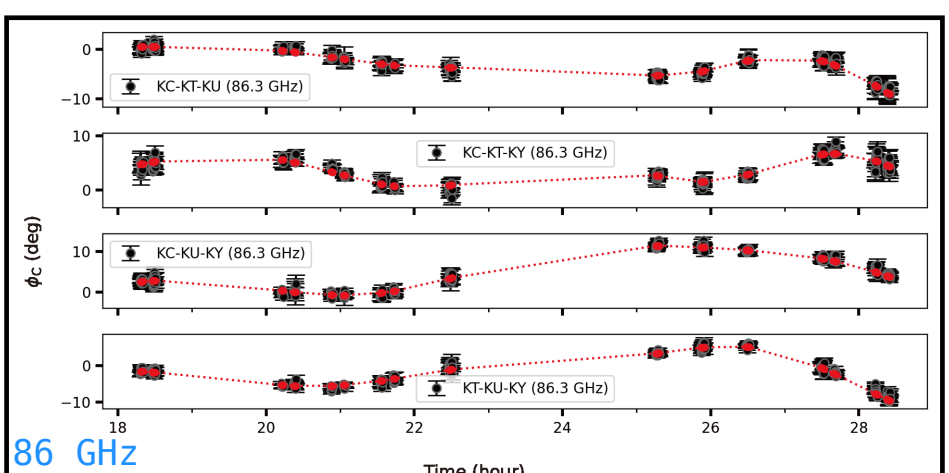

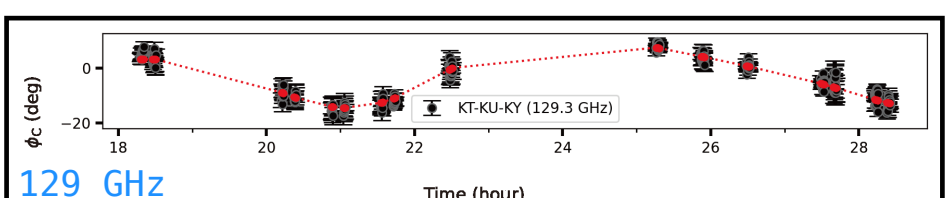

Simulation // gain calibration (supplementary)

100 simulations with random gain offset,
on two declinations –5deg & 40deg

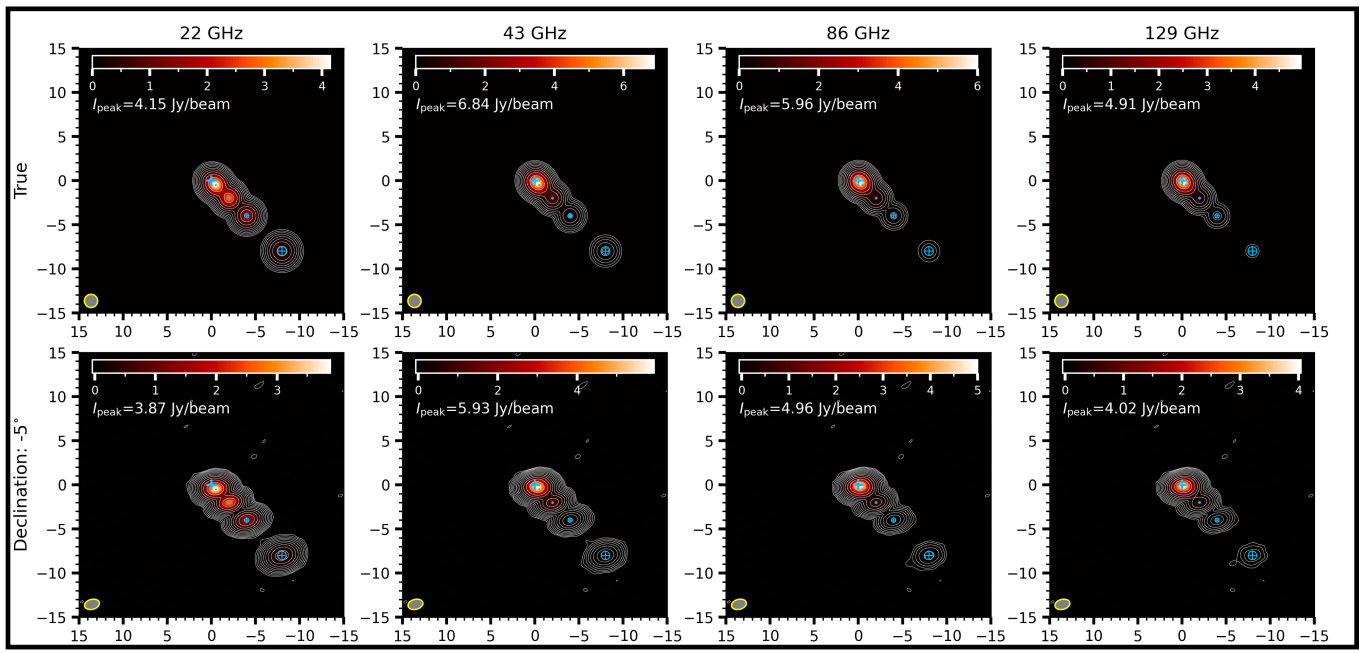

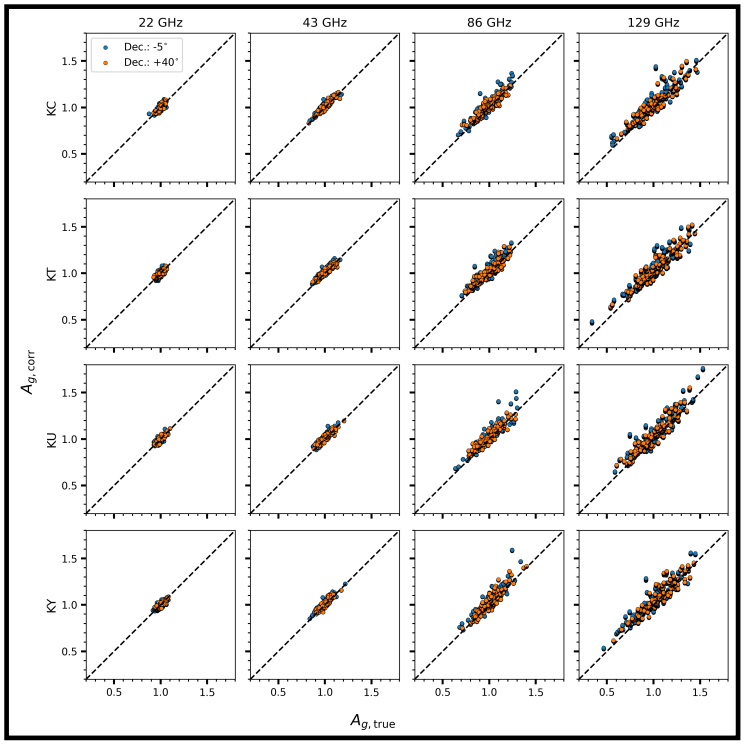

gain calibration results

–5 deg
+40 deg

Simulation // posterior distributions (supplementary)

100 simulations with random gain offset,
on two declinations −5deg & 40deg

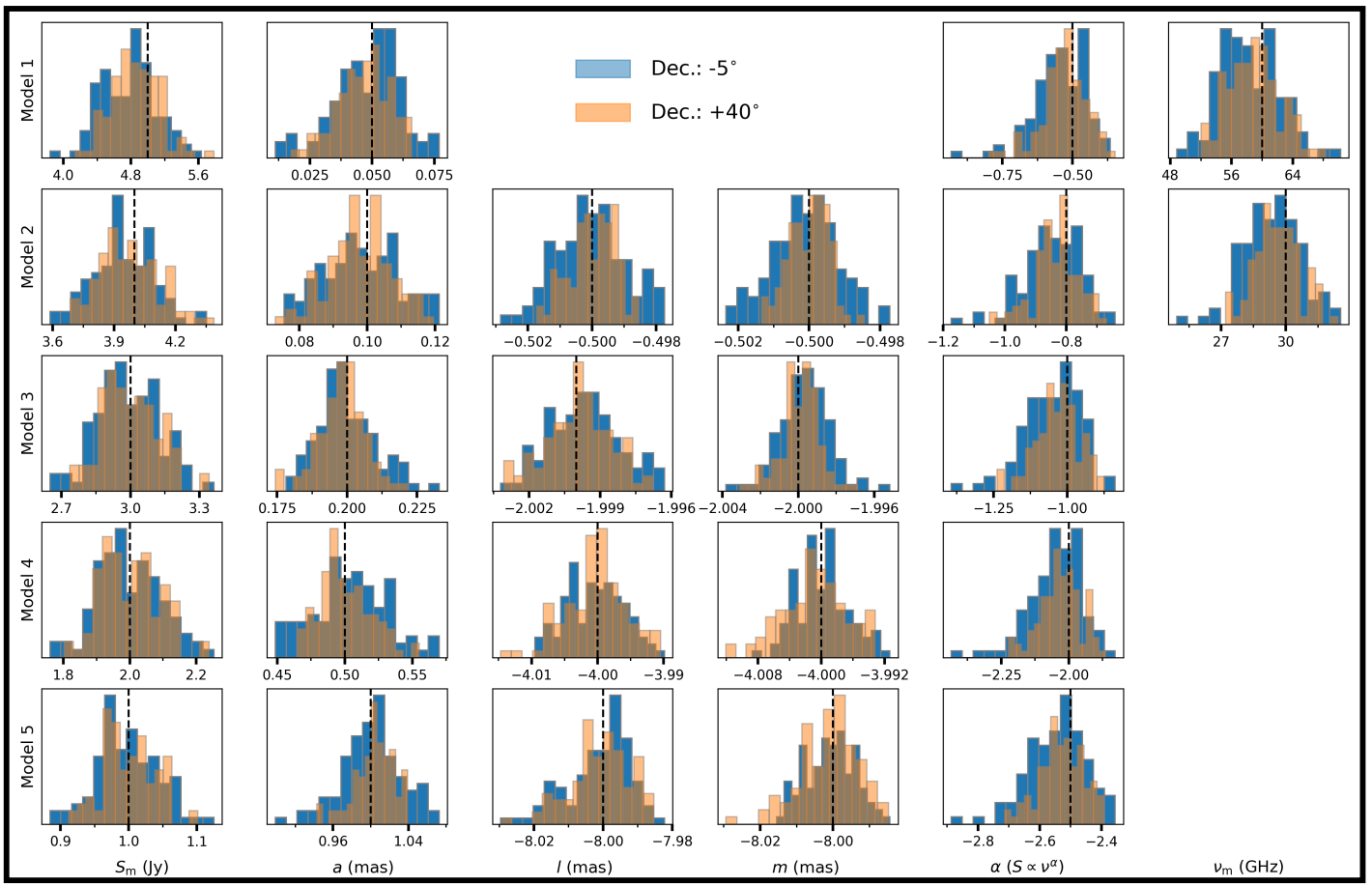

* black dashed lines: true value

Absolute EVPA calibration // n25hj01b, 2025-03-18 (supplementary)

Aligned EVPA of 3C 454.3

Polarimetry of 3C 454.3
obtained from a decadal monitoring of the KVN (Jeong+2025)

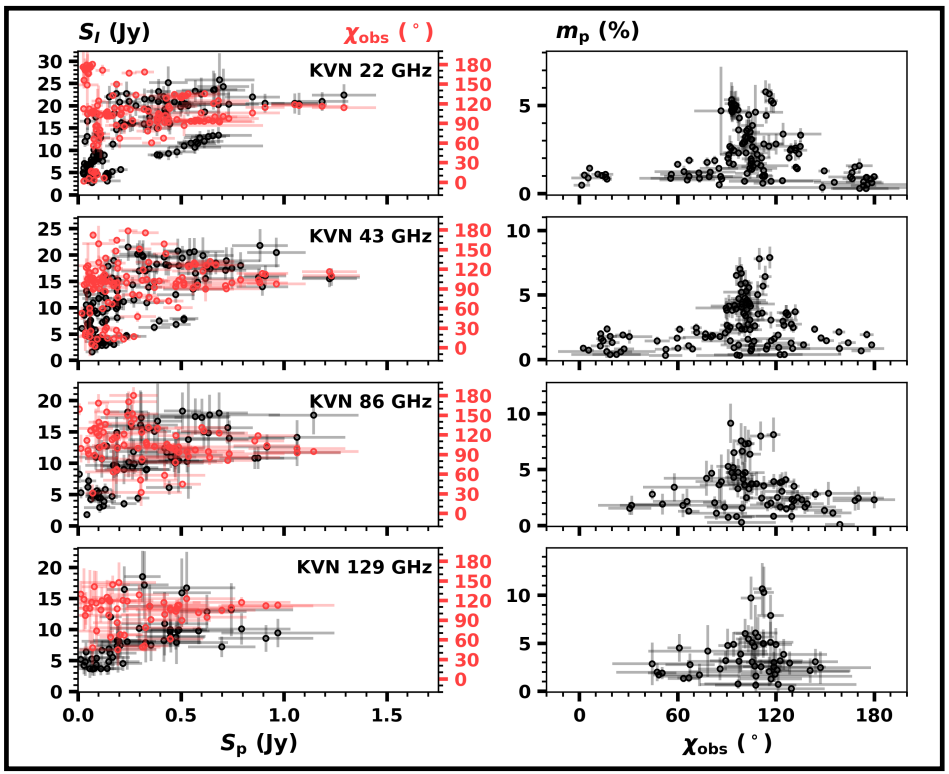

→ EVPA of this tends to be aligned at 90 – 100 deg, when highly polarized

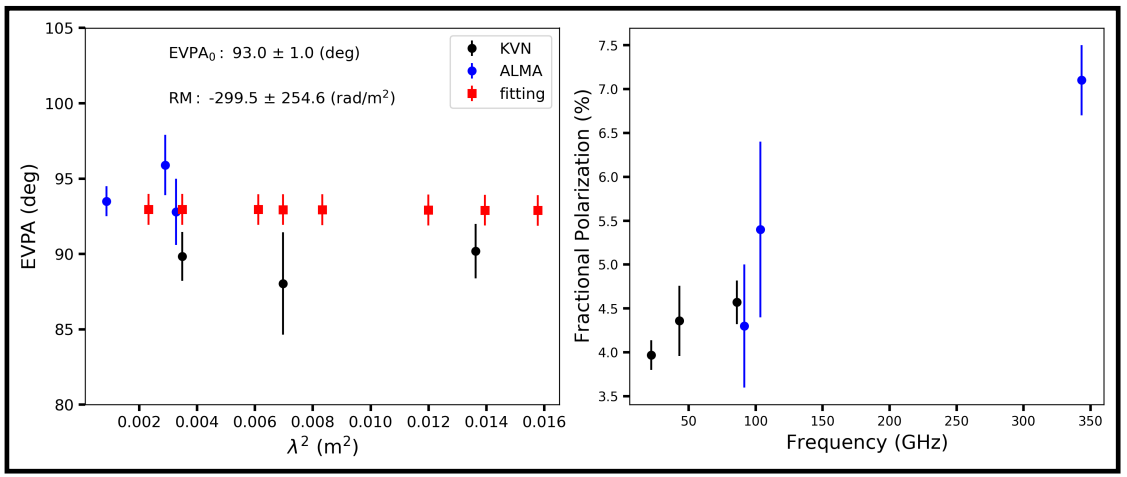

Polarimetry of 3C 454.3 in March 2025,
obtained from KVN (22 – 86 GHz) and ALMA (91 – 340 GHz)

* NOTE:
errors on the KVN data does not involve systematic uncertainties